Additive Manufacturing: Metallurgy, Cut Analysis & Porosity

12 Advanced Optical Metrology

Additive Manufacturing:
Metallurgy, Cut Analysis & Porosity

EVIDENT
OLYMPUS

WILEY

The latest eBook from Advanced Optical Metrology. Download for free.

In industry, sector after sector is moving away from conventional production methods to additive manufacturing, a technology that has been recommended for substantial research investment.

Download the latest eBook to read about the applications, trends, opportunities, and challenges around this process, and how it has been adapted to different industrial sectors.

EVIDENT
OLYMPUS

WILEY

RESEARCH ARTICLE

Antibacterial Films Based on MOF Composites that Release Iodine Passively or Upon Triggering by Near-Infrared Light

*Xu Han, Gerard Boix, Mateusz Balcerzak, Oscar Hernando Moriones,
Mary Cano-Sarabia, Pilar Cortés, Neus Bastús, Victor Puntes, Montserrat Llagostera,
Inhar Imaz,* and Daniel Maspoch**

Multidrug-resistant bacteria have become a global health problem for which new prophylactic strategies are now needed, including surface-coatings for hospital spaces and medical equipment. This work reports the preparation and functional validation of a metal-organic framework (MOF) based composite for the triggered controlled release of iodine, an antimicrobial element that does not generate resistance. It comprises beads of the iodophilic MOF UiO-66 containing encapsulated gold nanorods (AuNRs) coated with a silica shell. Irradiation of the AuNRs with near-infrared light (NIR) provokes a photothermal effect and the resultant heat actively liberates the iodine. After validating the performance of this composite, it is integrated into a polymer for the development of antibacterial films. This work assesses the adsorption of iodine into these composite films, as well as its passive long-term release and active light-triggered. Finally, this work validates the antibacterial activity of the composite films in vitro against gram-positive and gram-negative bacteria. The findings will surely inform the development of new prophylactic treatments.

X. Han, G. Boix, M. Balcerzak, O. H. Moriones, M. Cano-Sarabia,
N. Bastús, V. Puntes, I. Imaz, D. Maspoch
Catalan Institute of Nanoscience and Nanotechnology (ICN2)
CSIC and The Barcelona Institute of Science and Technology
Campus UAB, Bellaterra, Barcelona 08193, Spain
E-mail: inhar.imaz@icn2.cat; daniel.maspoch@icn2.cat
M. Balcerzak
Institute of Materials Science and Engineering
Poznan University of Technology
Jana Pawła II No 24, Poznan 61–138, Poland
O. H. Moriones
Universitat Autònoma de Barcelona (UAB)
Campus UAB, Bellaterra, Barcelona 08193, Spain
P. Cortés, M. Llagostera
Departament de Genètica i Microbiologia
Universitat Autònoma de Barcelona
Campus de Bellaterra, Cerdanyola del Vallès 08193, Spain
V. Puntes
Fundacio Hospital Universitari Vall D'Hebron – Institut De Recerca
08035, Passeig Vall D Hebron, Barcelona 119–129, Spain
V. Puntes, D. Maspoch
ICREA
Pg. Lluís Companys 23, Barcelona 08010, Spain

1. Introduction

Infectious diseases are a rapidly growing threat to humanity. For instance, the current COVID-19 pandemic, caused by the virus SARS-CoV-2, has already killed over 37 60 000 people[1] and is taking a devastating socioeconomic toll worldwide. Unfortunately, COVID-19 is only one of countless pathogenic diseases putting public health at risk. A particularly menacing group of such diseases is the nosocomial infections (also called *hospital-acquired infections*), which are caused by bacteria, viruses, fungi, yeast, or parasites acquired in hospital by a patient who was admitted for a reason other than that infection.[2] Nosocomial infections, which are facilitated primarily via urinary catheters, are a major cause of death and increased morbidity among patients, causing 1 10 000 deaths every year in Europe.[3,4]

Although bacterial and fungal infections can be treated with antibiotics, increased and inappropriate use of antibiotics has led to the emergence of highly menacing, multidrug-resistant bacteria. Accordingly, antimicrobial coatings of hospital surfaces and medical equipment are garnering increasing interest as a simple prophylactic strategy.[5] Such coatings impede the arrival and growth of microorganisms on surfaces, and maintain their inhibitory or destructive activity against transitory microorganisms after each use, thereby lowering the probability of future infections resulting from surface-contact. Typically, they are fabricated by incorporating biocides into polymers or hydrogels, which are subsequently released in a controlled fashion. In many of the antimicrobial coatings used today, the biocide is silver nanoparticles (NPs),[6] silver salts,[7] metal-oxide NPs,[8] antibiotics,[9] or quaternary ammonium compounds.[10] However, each of these current technologies suffers from certain limitations. For instance, silver-based coatings, which are popular because they have been widely characterized and demonstrate impressive in vitro performance, actually exhibit low microbial efficacy under real conditions.[11] Finally, quaternary ammonium coatings have demonstrated to be efficient, acting by disrupting the cytoplasmic and outer membrane lipid bilayers of bacteria; however, its performance can be reduced depending on the surface conditions (e.g., pH, presence of organic soil, hardness of water, and presence of blood).[11]

Among the most efficient topical biocides is iodine, which is widely available, inexpensive, and has broad-spectrum

**ADVANCED
SCIENCE NEWS**

www.advancedsciencenews.com

**ADVANCED
FUNCTIONAL
MATERIALS**

www.afm-journal.de

antimicrobial activity.[12] Furthermore, it works by causing irreversible, nonspecific damage to microorganism cells; thus, unlike antibiotics, it does not lead to resistance.[13] However, the low aqueous solubility of iodine limits its use in many applications. Moreover, although iodine is much more soluble in alcohols, these solvents permeate tissue too rapidly, causing over-administration of the iodine, which in turn leads to irritation and other undesirable side effects.[14] Since 1955, a water-based complex of polyvinylpyrrolidone (PVP) and iodine (also known as povidone-iodine; sold as Betadine, Inadine, and Braunol) has been the dominant formulation of iodine for topical antimicrobial use. Iodine is also widely used in dental/prosthetic implants, in which it is electrochemically absorbed into titanium.[15] However, despite the many advantages of iodine, the aforementioned challenges of solubility and release have precluded its use in antimicrobial films and coatings.[16]

Reflecting on approaches to circumvent the limitations of using iodine solutions directly in antimicrobial surface applications, we envisioned that adsorption of iodine into porous materials could enable both its storage and subsequent release, while preventing direct contact with human skin. Furthermore, we imagined that the resultant porous material could then be incorporated into polymeric matrices to yield antimicrobial films or coatings. Among the various types of porous materials available to store iodine, we reasoned that metal-organic frameworks (MOFs) would be ideal. Indeed, MOFs show high porosity, good thermal and chemical stability, and tunable pore size, shape, and functionality, all of which would facilitate selective adsorption and storage of iodine at loading capacities higher than the mass of the host MOF. For instance, the archetypical MOFs HKUST-1 and ZIF-8 have shown iodine uptake capacities of 1.75 mg mg$^{-1}_{MOF}$ and 1.25 mg mg$^{-1}_{MOF}$, respectively.[17–19] Once adsorbed into MOFs, iodine can then be released into solution.[20–22] Furthermore, many studies have confirmed that MOFs can be efficiently incorporated into organic polymer films to form mixed matrix-membranes, self-folding films, and other types of functional films.[23–27]

Interestingly, MOFs can be designed to undergo triggered release of adsorbed species via stimuli such as pH or light.[28–30] For example, a pH change that causes MOF degradation has been used to release hosted drugs (e.g., doxorubicin and artemisinin) from the well-known MOFs ZIF-8 and MIL-100(Fe). Alternatively, visible light has been used to provoke degradation of a Zr-based MOF via isomerization of its azobenzenedicarboxylate linker, thereby liberating its cargo.[31] Photoactive nanomaterials such as polypyrrole[32] and metal NPs[33,34] have also been combined with MOFs to generate composites that release their cargo upon exposure to visible or near-infrared (NIR) light.

Herein, we report the design, synthesis, and in vitro validation of antibacterial activity of MOF-based composite films that adsorb and store iodine at very high concentrations, and can release it in two ways: slowly and passively at low concentration; or, upon triggering by NIR light, rapidly and actively at high concentration. This composite is made of a spherical microbead of the MOF UiO-66 that encapsulates gold nanorods (AuNRs) coated with a silica shell (SiO$_2$) (hereafter called AuNR@SiO$_2$@UiO-66) (**Figure 1**a). The microporous UiO-66 adsorbs and stores iodine (at concentrations of up to

0.9 mg$_{I2}$ mg$_{composite}^{-1}$), whereas the photoactive AuNR@SiO$_2$ enables the active NIR-triggered release. Moreover, we demonstrate that these AuNR@SiO$_2$@UiO-66 microbead composites can be incorporated into organic polymers for developing iodine-based antimicrobial films that retain the iodine adsorption capacity and both release mechanisms. We validated the antibacterial activity of our light-responsive films against gram-positive and gram-negative bacteria.

2. Results and Discussion

2.1. Materials Synthesis and Characterization

AuNRs were prepared following a modified literature procedure.[35] Thus, a gold seed solution was initially prepared following the traditional cetyltrimethylammonium bromide (CTAB) stabilized synthesis.[35] The synthesized seeds were then placed into a growth solution with trace amounts of AgNO$_3$, and left overnight to develop into AuNRs. The synthesized rods were washed with Mili-Q water upon centrifugation. Field-emission scanning electron microscopy (FE-SEM), transmission electron microscopy (TEM) and UV-Vis spectroscopy revealed the formation of AuNRs with dimensions (length × width) of ≈80 × 15 nm (aspect ratio, AR = 5) (Figure S1a,d, Supporting Information), and with a maximum localized surface plasmon resonance (LSRP) peak at 810 nm (Figure S1e, Supporting Information). The AuNRs were coated with a silica shell following a modified Stöber process through a slightly adapted versions reported.[36–38] Briefly, a dispersion of synthesized AuNRs in a diluted CTAB solution (pH = 10) was reacted overnight with tetraethyl orthosilicate (TEOS) in the presence of 0.1 M of a sodium hydroxide solution as a catalyst in a methanolic solution. The resulting AuNRs coated with a silica shell (AuNR@SiO$_2$) of a thickness of 17 ± 2 nm (Figure S1b, Supporting Information) were centrifuged, and then thoroughly washed with ethanol. Finally, the silica shell thickness of AuNR@SiO$_2$ was increased by dispersing them in an ethanolic solution of ammonia and TEOS under mild stirring. The final AuNR@SiO$_2$ had an Au content of 23% and a shell thickness of 30 ± 3 nm, as confirmed by inductively coupled plasma-mass spectrometry (ICP-MS), FE-SEM, and scanning transmission electron microcopy (STEM) (Figure 1a, Figure S1c, Supporting Information). Importantly, this SiO$_2$ coating was required to prevent degradation of the AuNRs upon exposure to iodine: in previous studies, we noticed that naked AuNRs encapsulated in UiO-66 crystals were not stable to iodine at 75 °C, and that they became etched even after only brief exposure (Figure S2a, Supporting Information).[39] To this end, a coating thickness of around 30 nm of SiO$_2$ was found to be optimal for protection (Figure S2b, Supporting Information).

Next, we synthesized the AuNR@SiO$_2$@UiO-66 composite microbeads following a spray-drying methodology previously reported by our group (Figure 1a).[40] In a typical synthesis, a dispersion of AuNR@SiO$_2$ and the UiO-66 precursors (terephthalic acid and zirconium (IV) propoxide) dissolved in *N,N*-dimethylformamide (DMF) was injected into a coil-preheater, and then spray-dried at 180 °C. The synthesis was repeated without AuNR@SiO$_2$ to afford pristine UiO-66 microbeads.
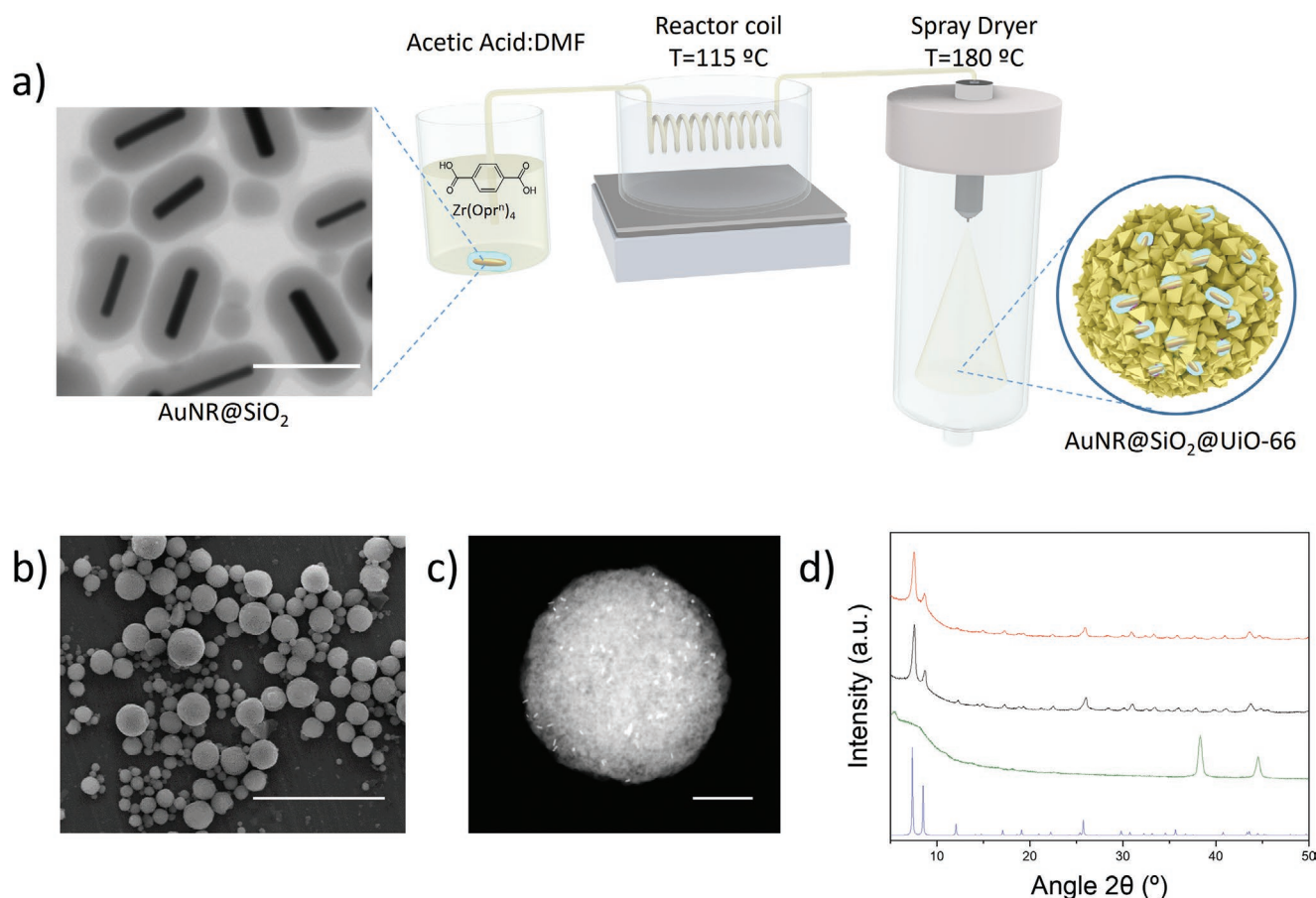
Figure 1. a) Schematic illustration of the spray-drying synthesis of AuNR@SiO₂@UiO-66 microbeads, using AuNRs coated with a SiO₂ shell (transmission electron microscopy, TEM image). b,c) Representative field-emission scanning electron microscopy (FE-SEM) (b) and high-angle annular dark-field scanning transmission electron microcopy (HAADF-STEM) (c) of AuNR@SiO₂@UiO-66 microbeads. d) Powder X-ray diffraction (PXRD) for simulated UiO-66 (blue), AuNR@SiO₂ (green), UiO-66 microbeads (black), and AuNR@SiO₂@UiO-66 microbeads (red). Scale bars: 100 nm (a), 20 μm (b), and 1 μm (c).

Powder X-ray diffraction (PXRD) and FE-SEM revealed the formation of spherical microbeads of both UiO-66 and AuNR@SiO₂@UiO-66 (Figure 1b,d). Moreover, the successful encapsulation of AuNR@SiO₂ in UiO-66 microbeads was confirmed by high-angle annular dark-field (HAADF-STEM) imaging (Figure 1c). The content of Au in the composite microbeads was estimated by first digesting them in an 8:3 mixture of 70% HNO₃ and HF at 230 °C, and then analyzing the byproducts by ICP-MS, from which an AuNR@SiO₂ content of 9% was determined. Nitrogen isotherm adsorption measurements revealed BET surface areas of 1040 m² g⁻¹ for the UiO-66 microbeads and 750 m² g⁻¹ for the AuNR@SiO₂@UiO-66 microbeads (Figure S3, Supporting Information). Note that this latter value is close to the expected value (946 m² g⁻¹), as calculated based on the loading percentage of AuNR@SiO₂ within the AuNR@SiO₂@UiO-66 microbeads.

Once we had synthesized the AuNR@SiO₂@UiO-66 microbeads, we studied their photothermal properties to ascertain their potential utility as a photoactivatable system for release of iodine. To this end, UiO-66 and AuNR@SiO₂@UiO-66 microbeads were separately irradiated

with NIR light (λ = 810 nm) at increasing intensity (52, 224, and 1000 mW cm⁻²) and the temperature was monitored using a thermal camera (Table S1, Supporting Information). The pristine UiO-66 microbeads did not respond photothermally to the NIR light; their temperature remained constant throughout the irradiation. Contrariwise, the AuNR@SiO₂@UiO-66 microbeads heated up rapidly (in less than 60 s; Figure S4, Supporting Information): at an intensity of 52 mW cm⁻², up to 90 °C; at 224 mW cm⁻², up to 150 °C; and finally, at 1000 mW cm⁻², up to 274 °C. Remarkably, they also cooled down just as quickly, as demonstrated once the NIR light had been turned off. This property of equivalently rapid heating and cooling is critical for precise switching (on/off) of triggered release.

2.2. Adsorption and NIR-Light Triggered Release of Iodine

We then determined the iodine-uptake capacity of the pristine UiO-66 microbeads and the composite AuNR@SiO₂@UiO-66, using a solid–gas adsorption setup. The sublimation chamber comprised two glass tubes of known mass, sealed at one end,
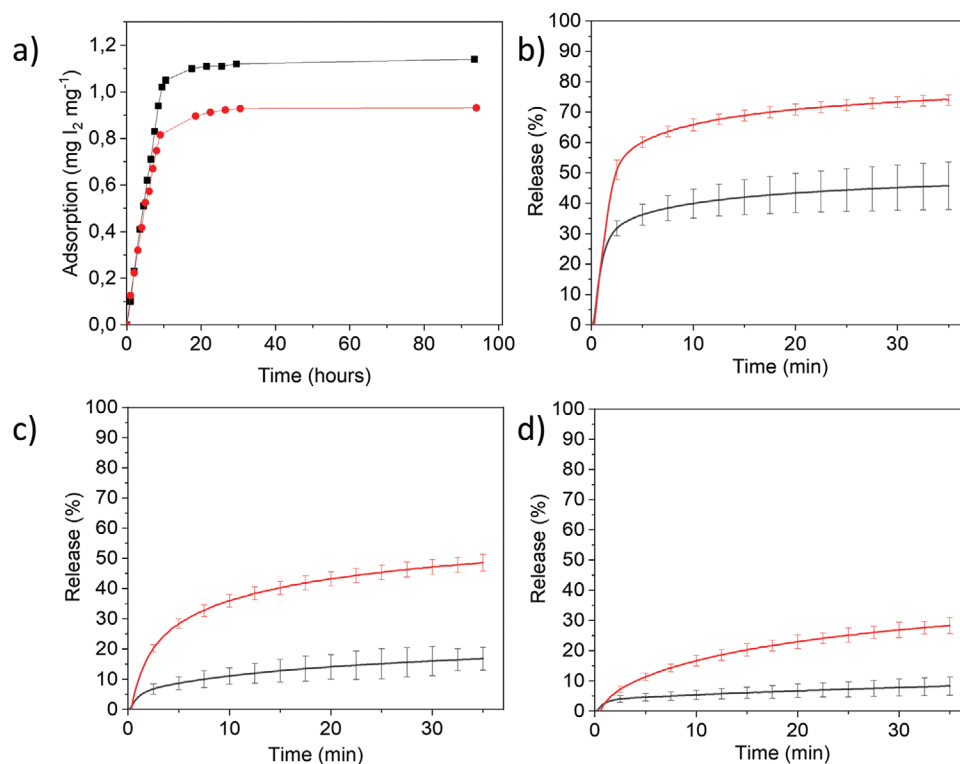
Figure 2. a) Iodine-adsorption isotherm at 75 °C for both UiO-66 (black) and AuNR@SiO$_2$@UiO-66 (red) microbeads. b–d) Iodine-release profiles for UiO-66 (black) and AuNR@SiO$_2$@UiO-66 (red) microbeads as triggered by near-infrared light (NIR) light at intensities of 1000 mW cm^{-2} (b), 224 mW cm^{-2} (c), and 52 mW cm^{-2} (d).

and placed inside a scintillation vial, into which the microbeads and the elemental iodine were separately introduced. Next, the sublimation chamber was purged with Ar gas to evacuate any humidity that could induce errors in gravimetric measurements, and the vial was placed inside an oven preheated to 75 °C. The optimum loading time was determined by periodically removing a sample of UiO-66 microbeads from the oven at different time intervals and carefully weighing the glass tube containing it. This experiment was also repeated with a sample of AuNR@SiO$_2$@UiO-66 microbeads. The resulting isothermal curves revealed a linear adsorption of iodine for the first 10 h, followed by saturation and finally, plateau of the adsorption after 20 h (**Figure 2**a). The exact uptake of iodine was confirmed by gravimetric experiments of samples after 20 h of adsorption, revealing a maximum uptake of 1.1 mg$_{I2}$ mg$_{composite}^{-1}$ for the pristine UiO-66 microbeads, and of 0.9 mg$_{I2}$ mg$_{composite}^{-1}$ for the composite AuNR@SiO$_2$@UiO-66 microbeads (Figure S5, Supporting Information). PXRD and HAADF-STEM imaging of UiO-66 microbeads and AuNR@SiO$_2$@UiO-66 microbeads loaded with iodine did not reveal any signs of material degradation (Figure S6, Supporting Information).

Next, we studied the NIR light-triggered release of iodine using a custom setup inside a thermogravimetric analyzer. To this end, I$_2$@UiO-66 and I$_2$@AuNR@SiO$_2$@UiO-66 microbeads were placed inside the unit, allowed to stand undisturbed for 5 min to stabilize their weight, and finally, irradiated (at 52, 224, and 1000 mW cm^{-2}) for 35 min. During irradiation, the weight of the microbeads was recorded to detect the loss of iodine. As expected, upon NIR irradiation,

the composite of I$_2$@UiO-66 microbeads with encapsulated AuNR@SiO$_2$ showed greater iodine-release than did the I$_2$@UiO-66 (Figure 2b–d) microbeads alone. Thus, for I$_2$@AuNR@SiO$_2$@UiO-66, the iodine-release values were 28% (0.26 mg$_{I2}$ mg$_{composite}^{-1}$) at 52 mW cm^{-2} irradiation; 48% (0.44 mg$_{I2}$ mg$_{composite}^{-1}$) at 224 mW cm^{-2}; and 74% (0.67 mg$_{I2}$ mg$_{composite}^{-1}$) at 1000 mW cm^{-2}. In contrast, for I$_2$@UiO-66, the values were 8% (0.09 mg$_{I2}$ mg$_{composite}^{-1}$) at 52 mW cm^{-2} irradiation; 16% (0.18 mg$_{I2}$ mg$_{composite}^{-1}$) at 224 mW cm^{-2} irradiation; and 45% (0.49 mg$_{I2}$ mg$_{composite}^{-1}$) at 1000 mW cm^{-2} irradiation. Note that, although I$_2$@UiO-66 released much less iodine than what I$_2$@AuNR@SiO$_2$@UiO-66 did upon NIR irradiation, it did release more iodine than expected, given the negligible photothermal properties of pristine UiO-66. This can be attributed to the intrinsic photothermal properties of iodine, which led to I$_2$@UiO-66 being heated up to 44 °C, when irradiated at 52 mW cm^{-2}; 90 °C, at 224 mW cm^{-2}; and 120 °C, at 1000 mW cm^{-2}. For comparison, iodine-release from the corresponding samples without NIR irradiation was also recorded. Without irradiation, the iodine-loss for I$_2$@AuNR@SiO$_2$@UiO-66 microbeads was 3% (0.025 mg$_{I2}$ mg$_{composite}^{-1}$) and for the I$_2$@UiO-66 microbeads, 4% (0.034 mg$_{I2}$ mg$_{composite}^{-1}$) (Figure S7, Supporting Information).

2.3. Integration of Au@SiO$_2$@UiO-66 Microbeads into PVDF Films

Having confirmed the NIR-triggered release of iodine from our I$_2$@AuNR@SiO$_2$@UiO-66 microbeads, we then sought
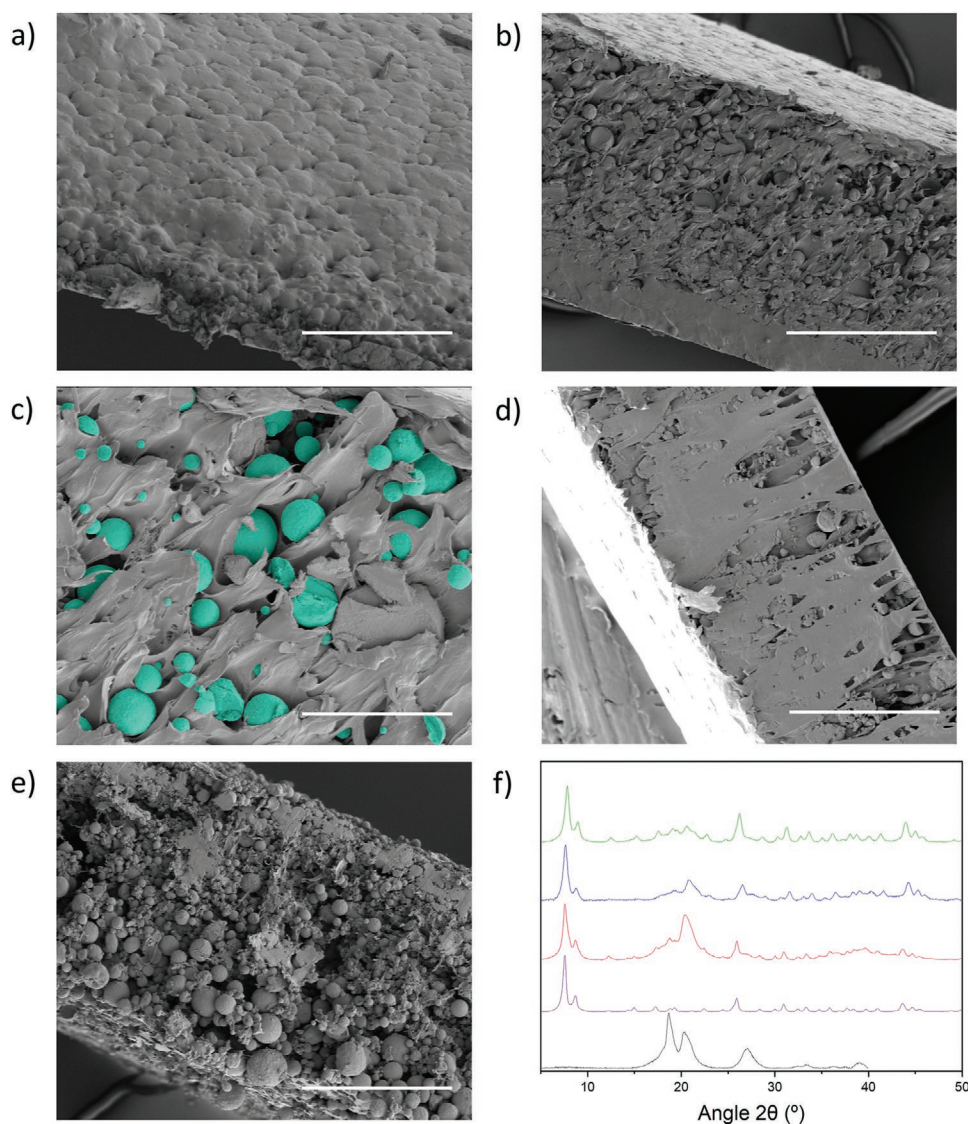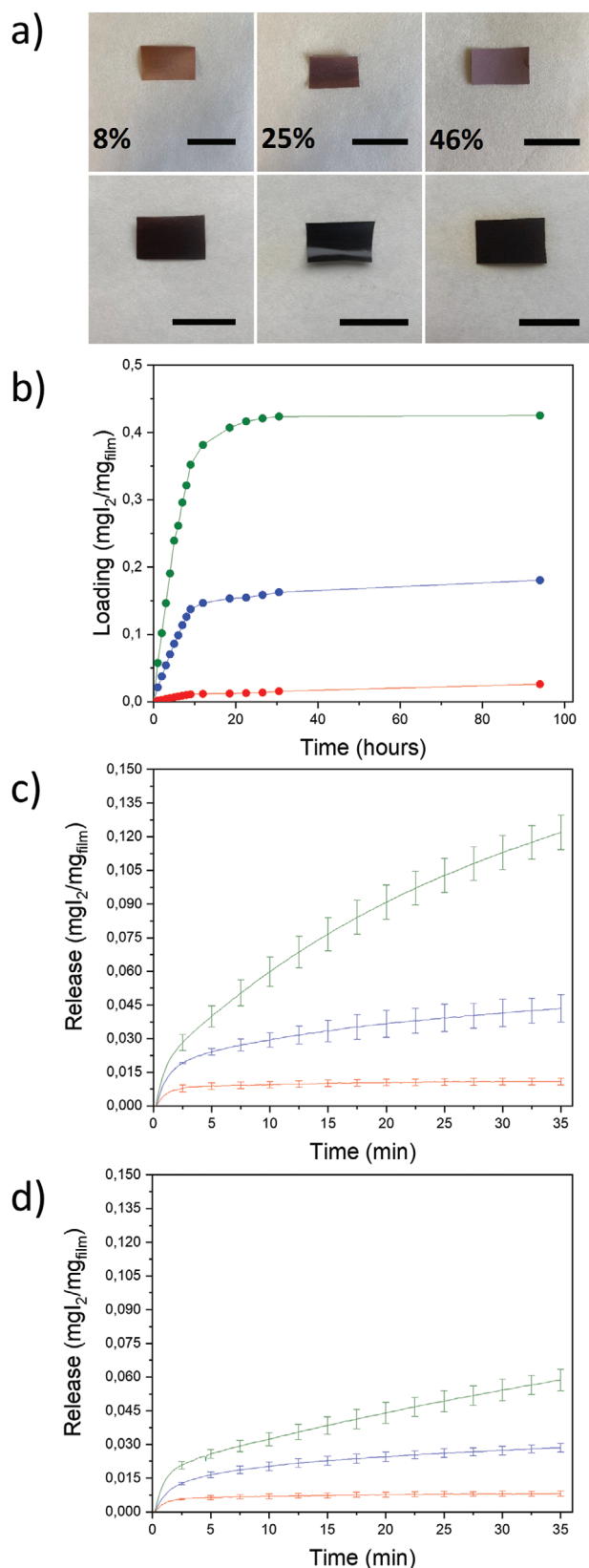
Figure 3. a-c) Field-emission scanning electron microscopy (FE-SEM) of the cross-section of the films containing AuNR@SiO$_2$@UiO-66 microbeads at 25% (w/w). In (c), the microbeads are highlighted in pale green to better illustrate encapsulation of them. d,e) FE-SEM of the cross-section of the films containing AuNR@SiO$_2$@UiO-66 microbeads at 8% (d) or 46% (e) (w/w). f) Powder X-ray diffraction (PXRD) of a pristine polyvinylidene difluoride (PVDF) film (black), AuNR@SiO$_2$@UiO-66 microbeads (purple), and films containing AuNR@SiO$_2$@UiO-66 microbeads at 8% (red), 25% (blue) or 46% (green) (w/w). Scale bars: 200 μm (a), 50 μm (b), 5 μm (c), 50 μm (d), and 50 μm (e).

to integrate them into a polymeric film, with the ultimate aim of fabricating a coating for antibacterial applications in which sterilization could be selectively triggered. To this end, AuNR@SiO$_2$@UiO-66 microbeads were encapsulated into a polyvinylidene difluoride (PVDF) film using a previously reported procedure.[25] In a typical synthesis, the necessary amount AuNR@SiO$_2$@UiO-66 microbeads [10%, 30% and 50% (w/w)] were dispersed in a PVDF solution in DMF and drop-cast onto a glass surface. The DMF was evaporated off by placing the glass slide in an oven (140 °C) for 30 min. The fabricated films were then thoroughly washed with methanol and finally, dried under vacuum overnight. For comparison, a PVDF film without AuNR@SiO$_2$@UiO-66 microbeads also was prepared by the method. FE-SEM imaging of the cross-section of each film revealed a thickness of 140 μm (**Figure 3**a), in which the

AuNR@SiO$_2$@UiO-66 microbeads retained their morphology and were homogeneously dispersed throughout (Figure 3b–e, Figure S8, Supporting Information). Moreover, PXRD analysis of the three films containing the microbeads revealed that their crystalline structure had not been affected during film formation (Figure 3f). Quantification of the exact mass percentage of AuNR@SiO$_2$@UiO-66 microbeads inside the films by ICP-MS analysis revealed values of 8%, 25%, and 46% (w/w) for the films fabricated with 10%, 30%, and 50% (w/w) of microbeads, respectively.

To evaluate the iodine-uptake capacity of the three composite films (**Figure 4**a), we started by measuring the capacity of a section (2 cm^2) of the bare film (i.e., film lacking microbeads) to adsorb iodine using the same procedure as we described for the AuNR@SiO$_2$@UiO-66 microbeads, in which we quantified

**ADVANCED
SCIENCE NEWS**

www.advancedsciencenews.com

**ADVANCED
FUNCTIONAL
MATERIALS**

www.afm-journal.de

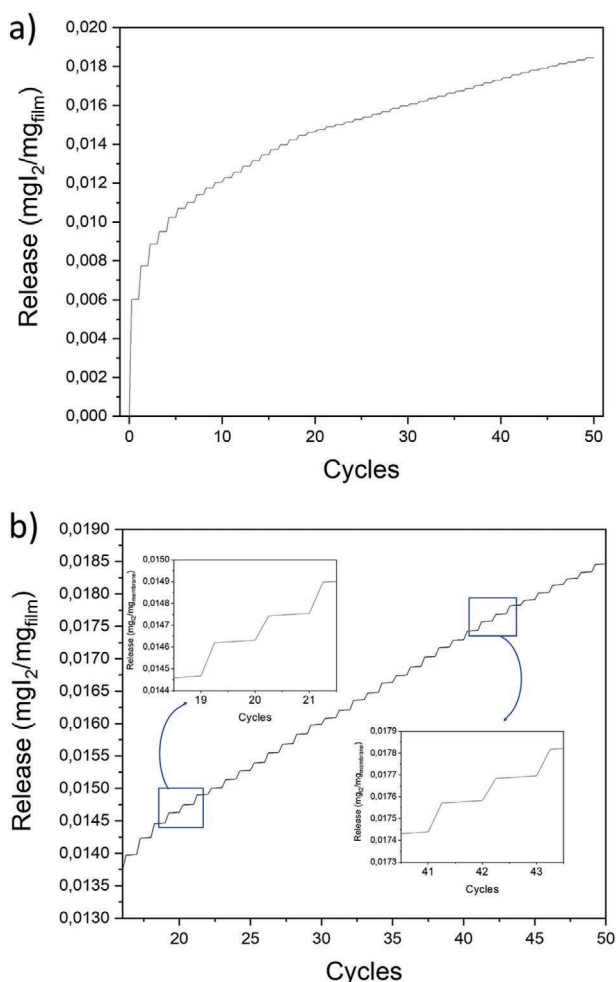**Figure 4.** a) Photographs of the composite films containing different concentrations of AuNR@SiO₂@UiO-66 microbeads before (top) and after (bottom) loading with iodine. Scale bar: 2 cm. b) Adsorption isotherm

the iodine-loading by thermogravimetric analysis (Figure S9, Supporting Information). The bare film barely adsorbed iodine (5×10^{-4} mg_{I_2} mg_{film}^{-1}). Contrariwise, for similar experiments performed on sections (2 cm²) of films loaded with microbeads, the following sorption capacities were observed, according to the maximum possible iodine adsorption of the AuNR@SiO₂@ UiO-66 microbeads within each film: at 8% microbead-loading, 0.012 mg_{I_2} mg_{film}^{-1} (17% of expected value [0.072 mg_{I_2} mg_{film}^{-1}]); at 25% loading, 0.159 mg_{I_2} mg_{film}^{-1} (71% of the expected value [0.225 mg_{I_2} mg_{film}^{-1}]); and at 46% loading, 0.434 mg_{I_2} mg_{film}^{-1} (105% of the expected value [0.414 mg_{I_2} mg_{film}^{-1}) (Figure 4b). These results confirm that AuNR@SiO₂@UiO-66 microbeads can adsorb iodine even when encapsulated into PVDF films and illustrate that the adsorption increases with increasing microbead loading. We attributed this behavior to the fact that, as the microbeads content increases, so does the number of interfacial voids formed between the polymer and composite beads, and consequently, so does the permeability. Interestingly, this phenomenon has already been described in MOF-based mixed-matrix membranes, in which the formation of interfacial voids arising from poor adhesion of the polymer matrix and porous filler particles are typically observed.[31] Moreover, microbead loading negatively correlates to the temperature required to fully desorb the iodine from the films: at 8% microbead-loading, that temperature is 240 °C; at 25%, 220 °C; and at 46%, 200 °C (Figure S9, Supporting Information). In fact, the final value is very close to that observed for the bare AuNR@SiO₂@ UiO-66 microbeads (190 °C), again corroborating a higher number of interfacial voids or greater hierarchical porosity in the composite films.

We then studied the triggered release of iodine from the three composite films by the same methodology that we previously used for I₂@AuNR@SiO₂@UiO-66 microbeads. To this end, the films containing microbeads at different loadings were independently placed inside the thermogravimetric analysis ((TGA) setup, allowed to stand undisturbed for 10 min to stabilize their weight, and finally, irradiated at 52 or 224 mW cm⁻² for 35 min, while iodine loss was recorded. Upon irradiation, the following values for maximum release of total loaded iodine were recorded: at 8% microbead-loading, 17% (0.002 mg_{I_2} mg_{film}^{-1}); at 25% microbead-loading, 18% (0.029 mg_{I_2} mg_{film}^{-1}); and at 46% microbead-loading, 17% (0.073 mg_{I_2} mg_{film}^{-1}) (Figure 4d). Alternatively, upon irradiation at 224 mW cm⁻², the corresponding recorded values were: at 8% microbead-loading, 28% (0.004 mg_{I_2} mg_{film}^{-1}); at 27% microbead-loading, 18% (0.044 mg_{I_2} mg_{film}^{-1}); and at 46% microbead-loading, 30% (0.121 mg_{I_2} mg_{film}^{-1}) (Figure 4c). In all these composite films, these results obtained represent nearly 63% of the expected release according to their contents of AuNR@SiO₂@UiO-66 microbeads. We rationalized the fact that less iodine was released from the composite films than from the pure AuNR@SiO₂@UiO-66 microbeads under the

of iodine at 75 °C for the films containing AuNR@SiO₂@UiO-66 microbeads at 8% (red), 25% (blue), or 46% (green) (w/w). c,d) Light-triggered iodine- release profiles for the films containing I₂@AuNR@SiO₂@UiO-66 microbeads at 8% (red), 25% (blue), or 46% (green) (w/w) under irradiation intensities of 224 mW cm⁻² (c) and 52 mW cm⁻² (d).

**ADVANCED
SCIENCE NEWS**

www.advancedsciencenews.com

**ADVANCED
FUNCTIONAL
MATERIALS**

www.afm-journal.de

Figure 5. a) Stepwise release of iodine from a composite film containing I$_2$@AuNR@SiO$_2$@UiO-66 microbeads at 25% (w/w) irradiated with near-infrared light (NIR) light at 52 mW cm^{-2} and subjected to on/off switching. b) Zoom on the stepwise release after its stabilization at the 15th cycle.

release via repetitive cycles of on/off switching. To this end, two portions of film containing 25% I$_2$@AuNR@SiO$_2$@UiO-66 microbeads were irradiated at 52 or 224 mW cm^{-2} for 1 min, after which the light was turned off for 3 min. This on/off cycle was ultimately repeated 50 times. At both intensities, the films demonstrated stepwise release of iodine via on/off switching (**Figure 5**a and Figure S11a, Supporting Information): turning the NIR light on released the iodine, but turning it off slowed the release down. The iodine release occurred in a burst in the first switching cycle (0.006 mg$_{I2}$ mg$_{film}^{-1}$ at 52 mW cm^{-2}; and 0.016 and at 224 mW cm^{-2}), decreased until reaching a plateau at the fifteenth cycle, and then stayed constant for the remaining cycles (9 × 10^{-5}–8 × 10^{-5} mg$_{I2}$ mg$_{film}^{-1}$ at 52 mW cm^{-2}; and 1.7 × 10^{-4}–1,6 × 10^{-4} mg$_{I2}$ mg$_{film}^{-1}$ at 224 mW cm^{-2}) (Figure 5b and Figure S11b, Supporting Information).

2.3.1. Antibacterial Activity

Having demonstrated the controlled release of iodine from the UiO-66 and AuNR@SiO$_2$@UiO-66 microbeads and composite films, we next ascertained their antibacterial activity, beginning with the disk-diffusion method. The UiO-66 microbeads and the AuNR@SiO$_2$@UiO-66 microbeads lacking iodine did not impair the growth of *Escherichia coli* (gram-negative bacterium) or *Staphylococcus aureus* (gram-positive bacterium), even under irradiation with NIR light. Contrariwise, UiO-66 microbeads and AuNR@SiO$_2$@UiO-66 microbeads loaded with iodine each led to well-defined inhibition growth zones, both with and without NIR irradiation. The diameters of the respective growth-inhibition zones were higher against *S. aureus* (31 to 33 mm) than against *E. coli* (24 to 26 mm). Interestingly, there were no significant differences between loaded I$_2$@UiO-66 or I$_2$@AuNR@SiO$_2$@UiO-66 products (Figure S12, Supporting Information). Notably, the growth-inhibition obtained with both types of materials were higher than that produced by povidone-iodine (common antiseptic with a broad spectrum of antimicrobial activity) at similar concentrations of iodine, for which the growth-inhibition zones had diameter against *S. aureus* was 10 mm and against *E. coli*, 7 mm (data not shown). Additionally, the composite films prepared at different iodine-containing microbead-loadings (8%, 25%, or 46%) and tested on *E. coli* cultures also produced inhibition zones, the diameters of positively correlated significantly ($p < 0.0001$) to iodine concentration (Figure S13 and Table S2, Supporting Information). These results demonstrated the capacity of iodine to be persistently released from UiO-66 or AuNR@SiO$_2$@UiO-66 microbeads, either in the solid-state or when incorporated in films, throughout the agar layer during overnight incubation at 37 °C. However, NIR irradiation did not enhance the antibacterial activity of the iodine-loaded I$_2$@AuNR@SiO$_2$@UiO-66 composites. We partially expected this behavior as, in these experiments, we only evaluated the antibacterial activity of iodine release through diffusion along the agar inoculated with bacterial suspensions: we did not assess the activity of the iodine released through the air passively or actively (i.e., via light-triggering).

To solve the aforementioned problem, and to evaluate the antibacterial performance of the composite films upon iodine release through the air by sublimation via both the passive and

same conditions according to the diffusion barrier generated by the polymeric films. Finally, and as in the earlier iodine-loss experiments, the iodine-loss in the absence of irradiation was recorded for comparison, for which the recorded values were: at 8% microbead-loading, 3.1% (4 × 10^{-4} mg$_{I2}$ mg$_{film}^{-1}$); at 25% microbead-loading, 3.3% (0.006 mg$_{I2}$ mg$_{film}^{-1}$); and at 46% microbead-loading, 4.1% (0.014 mg$_{I2}$ mg$_{film}^{-1}$).

Finally, without irradiation, the films containing microbeads at 25% or 46% (w/w) exhibited slow and prolonged release (Figure S10, Supporting Information), liberating ≈50% of their total iodine content over 2 months. This release was faster in the first month, after which the film at 25% microbead-loading released, on average, 2 × 10^{-4} mg$_{I2}$ mg$_{film}^{-1}$ iodine per day, and the film at 46% microbead-loading, 4 × 10^{-4} mg$_{I2}$ mg$_{film}^{-1}$ per day.

Once we had demonstrated that, even when I$_2$@AuNR@SiO$_2$@UiO-66 microbeads were incorporated into polymer films, they could still trigger the release of iodine upon NIR irradiation, we then explored the possibility of controlling this
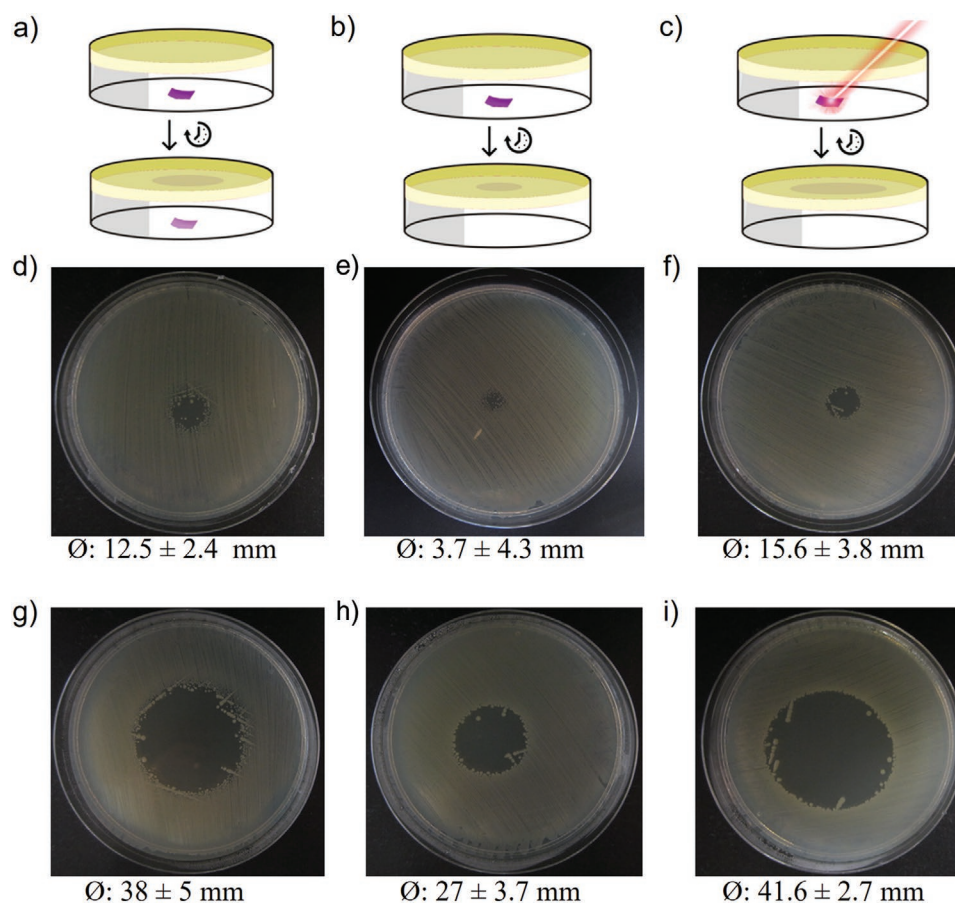
**ADVANCED
SCIENCE NEWS**

www.advancedsciencenews.com

**ADVANCED
FUNCTIONAL
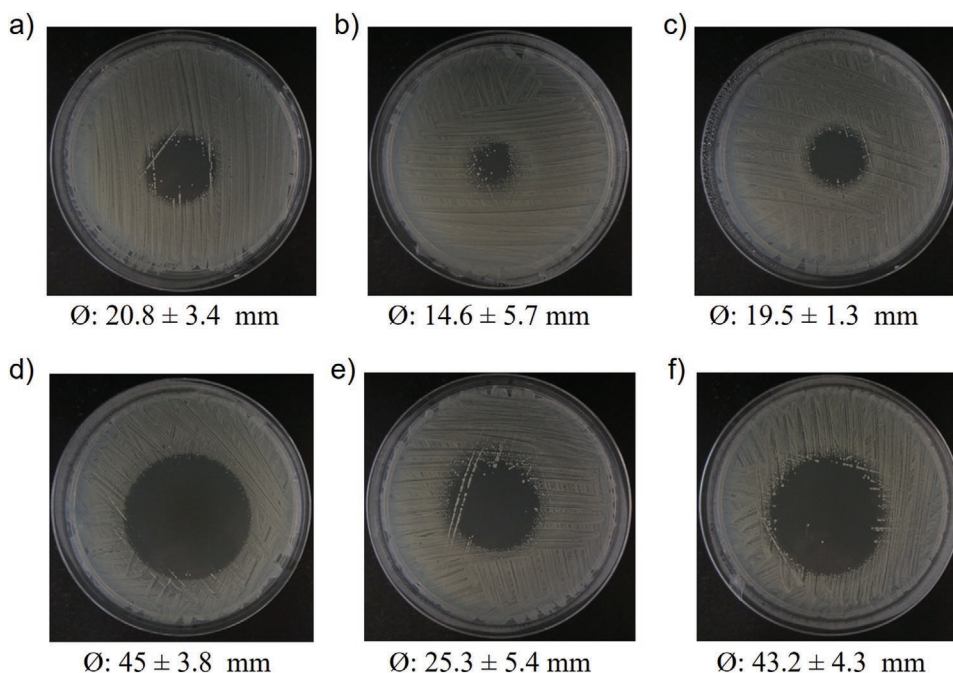MATERIALS**

www.afm-journal.de

Figure 6. a–c) Schematic illustrations of the three experiments performed to study the passive (a) or light-triggered (b,c) antibacterial performance of the composite films containing iodine-loaded I_2@AuNR@SiO$_2$@UiO-66 microbeads. d–i) Corresponding inhibition growth zones of *Escherichia coli* cultures produced in composite films containing microbeads at 8% (d–f) or 25% (g–i) (w/w). Left (d,g): photographs taken after co-incubation of both composite film and agar plate inoculated with *E. coli*. Center (e,h) and right (f,i): photographs taken after incubation of the agar plate inoculated with *E. coli* once the composite films had been removed. The composite films shown in (f,i) had been irradiated with near-infrared light (NIR) light. Ø: diameter of the growth-inhibition zone. Values are the average of at least four replicates ± standard deviation.

the light-triggered mechanisms, we designed a new experimental setup and performed multiple experiments with it. It comprised placing a 1 cm^2 portion of each composite film, containing iodine-loaded I_2@AuNR@SiO$_2$@UiO-66 microbeads at either 8% or 25%, over a plate cover, and then putting the agar plate inoculated with bacterial suspensions face down on the cover, such that the distance between the film and agar plate was fixed to 1.6 cm. Next, three different experiments were performed. In the first experiment, the two plates were co-incubated at 37 °C for 18 h to evaluate the antibacterial performance conferred by passive iodine release (**Figure 6**a). In the second, the composite film was irradiated with NIR light (intensity: 224 mW cm^{-2}) for 5 min. Then, the composite film was immediately removed, and the agar plate was sealed with parafilm and finally, incubated at 37 °C for 18 h (Figure 6c). The third experiment was similar to the second one, except that the film was not irradiated (Figure 6b). These last two experiments were designed to enable evaluation of the antibacterial performance conferred by the light-triggered release of iodine. In all cases, the corresponding control conditions using composite films without iodine and/or without irradiation also were tested.

In the above three experiments, we observed that passive release of iodine via sublimation inhibited the growth of both *E. coli* (Figure 6d,g) and *S. aureus* (**Figure 7**a,d). Moreover, we also observed that the light-triggered release of iodine inhibited the growth of both bacteria (Figure 6e,f,h,i, and Figure 7b,c,e,f). In all cases, the inhibition zones had a larger diameter in the irradiated experiments than in the nonirradiated ones. In *E. coli* cultures, these differences were statistically significant when the films containing 8% ($p = 0.0002$) and 25% microbeads ($p < 0.0001$) were irradiated and nonirradiated for 5 min and then removed. Regarding *S. aureus*, statistically results were obtained at 25% ($p < 0.0001$) (Tables S3 and S4, Supporting Information). This is in quite contrast to identical experiments performed with films that do not contain AuNR@SiO$_2$ NPs, in which the inhibition zones were similar in the irradiated and nonirradiated experiments (Figure S14, Supporting Information). Importantly, the antibacterial activity of the irradiated composite films also positively correlated with the content of iodine-loaded I_2@AuNR@SiO$_2$@UiO-66 microbeads. The film containing microbeads at 8% (w/w) exhibited greater antibacterial activity against *S. aureus* than against *E. coli*; however, this

**ADVANCED
SCIENCE NEWS**

www.advancedsciencenews.com

**ADVANCED
FUNCTIONAL
MATERIALS**

www.afm-journal.de

Figure 7. Growth-inhibition zones in *Staphylococcus aureus* cultures generated by composite films containing iodine-loaded I_2@AuNR@SiO_2@UiO-66 microbeads at 8% (a–c) or 25% (d–f) (w/w). Left (a,d): photographs taken after co-incubation of the composite film and an agar plate inoculated with *S. aureus*. Center (b,e) and right (c,f): photographs taken after incubation of an agar plate inoculated with *S. aureus*, after the composite films had been removed. The composite films shown in (c,f) had been irradiated with near-infrared light (NIR) light. Ø: diameter of the growth-inhibition zone. Values are the average of at least four replicates ± standard deviation.

difference was less pronounced for the film containing microbeads at 25% (w/w). Altogether, these results confirmed the effective passive, long-lasting antibacterial activity of our composite films against gram-positive and gram-negative bacteria and that this activity can be enhanced by irradiating the films with NIR light to trigger release of iodine.

3. Conclusions

We designed, synthesized, and validated for antibacterial activity in vitro, a MOF composite that can store iodine and then, release it two ways: either passively and slowly, or, upon triggering by NIR light, actively and quickly. The composite comprises SiO_2-coated AuNRs encapsulated within microbeads of the MOF UiO-66, which is then loaded with iodine and can be produced as thin films. The AuNR@SiO_2@UiO-66 composite was synthesized by a scalable, continuous-flow, spray-drying methodology, enabling facile and homogeneous distribution of the encapsulated photoactive AuNR@SiO_2 NPs throughout the microbeads. We found that the silica coating around the AuNRs was essential to synthesize a long-life composite, as bare AuNRs were degraded upon exposure to iodine. The microporous UiO-66 can adsorb and store iodine at concentrations of up to 0.9 mg_{I2} $mg_{composite}^{-1}$, and then release it either passively over time, or actively, upon irradiation with NIR light, which heats the composite to temperatures of up to 274 °C. Intriguingly, rapid heating and cooling of the AuNR@SiO_2@UiO-66 composite enabled stepwise release of iodine through selective on/off switching. Next, we showed that these

AuNR@SiO_2@UiO-66 microbeads could be incorporated at different concentrations into organic polymers to afford iodine-based antibacterial films that retain the iodine adsorption capacity, and dual release mechanisms, of the parent composite. Finally, the passive and light-triggered antibacterial performance of these composite films was confirmed against *S. aureus* (gram-positive) and *E. coli* (gram-negative), opening the way to develop new smart prophylactic coatings. We are confident that these encouraging findings on our iodine-loaded I_2@AuNR@SiO_2@UiO-66 composite and related thin films will inform future efforts at developing new iodine-based antibacterial materials designed to prevent nosocomial and other microbial infections, including coatings for medical instruments or hospital surfaces.

4. Experimental Section

Materials and Methods: Zirconium (IV) propoxide solution (70% (w/w)) in 1-propanol, terephthalic acid, gold(III) chloride hydrate, TEOS ≥ 99.0%, glacial acetic acid, sodium hydroxide, cetyltrimethylammonium bromide, sodium borohydride, silver nitrate, ascorbic acid, absolute ethanol ≥ 99.8%, and ammonium hydroxide 28% were purchased from Sigma Aldrich. *N,N*- DMF, methanol, ethanol, sulfuric acid, and acetone were purchased from Fisher Scientific. All the reagents were used without further purification. Deionized water, obtained with a Milli-Q system (18.2 MΩ cm), was used when required. PXRD patterns were collected on an X'Pert PRO MPDP analytical diffractometer (Panalytical) at 45 kV and 40 mA using CuKα radiation ($\lambda = 1.5419$ Å). Nitrogen adsorption and desorption measurements were collected at 77 K using an ASAP 2460 (Micromeritics). Temperature for N_2 isotherms measurement was controlled by using a liquid nitrogen

bath. FE-SEM images were collected on a Magellan 400 L scanning electron microscope (FEI) at an acceleration voltage of 5.0 KV. TEM images were collected on a Tecnai G2 F20 microscope (FEI) at 200 KV. ICP-MS experiments were performed on an Agilent 7500. Laser irradiation was performed using a Lasiris Powerline 810 (Coherent). Thermal imaging was obtained using a PI 450 (Optris) infrared camera. Inductively Coupled Plasma–Optical Emission Spectroscopy (ICP-MS) measurements were performed on an Agilent 7500. TGA experiments were run on a Perkin-Elmer-TGA-8000G, under N_2 atmosphere.

Synthesis of AuNRs: The AuNRs were synthesized through a seed-mediated growth procedure adapted from the literature.[35] In a typical synthesis, 273.4 mg of CTAB was dissolved in 7.5 mL H_2O inside a 15 mL scintillation vial under magnetic stirring. Next, 2 mL of a $HAuCl_4$ (24×10^{-3} M) solution was added, and the resultant mixture was stirred for 10 s. Afterwards, 0.6 mL of ice-cold aq. $NaBH_4$ (10×10^{-3} M) was added, and the mixture was stirred at 600 rpm for 2 min. Finally, the magnetic stir-bar was removed, and the seed solution was allowed to react for 3 h at 28 °C. In parallel, 437.4 mg CTAB was dissolved in 10 mL of H_2O inside a 20 mL scintillation vial under magnetic stirring. Then, sequentially, 204 μL of aq. $HAuCl_4$ (24×10^{-3} M), 0.2 mL of aq. H_2SO_4 (0.5 M), 75 μL of aq. $AgNO_3$ (0.01 M) and 80 μL of aq. ascorbic acid (0.1 M) were added into the solution, with 10 s of stirring between each addition. Next, 24 μL of the above-prepared seed solution was added into this solution, and the resultant mixture was vigorously stirred for 30 s. The magnetic stir-bar was removed, and the mixture was left to react at 28 °C for 12 h. Finally, the resulting AuNRs were separated through centrifugation, and then washed twice in Milli-Q water to remove any excess CTAB.

Coating of AuNRs with a Silica Shell: The AuNRs were coated with a silica shell following a slightly modified combination of reported procedures.[36–38] Thus, the synthesized AuNRs were dispersed in 10 mL of aqueous 0.6×10^{-3} M CTAB solution, and the resulting mixture was stirred for 12 h. The pH of the AuNR dispersion was then adjusted to 10.0 to 10.4 using aq. NaOH solution (0.1 M), and the mixture was stirred for 30 min. Afterwards, 90 μL of freshly prepared 20% (v/v) TEOS in methanol was added, and the resulting solution was stirred gently at 70 rpm for a further 30 min. Finally, the magnetic stir-bar was removed, and the reaction mixture was left at 28 °C overnight. The obtained silica-coated rods (hereafter named AuNR@SiO_2) were washed three times by centrifugation and redispersion in ethanol. The thickness of the silica-shell coating was confirmed by FE-SEM/TEM imaging to be 17 ± 2 nm. The silica coating was thickened following a modified Stöber process.[36] First, the AuNR@SiO_2 were concentrated into 2 mL of absolute ethanol and then they were redispersed under mild sonication. Later, AuNR@SiO_2 were placed into a 40 mL of absolute ethanol that contained 1.2 mL of ammonia NH_4OH (28%) and 200 μL of a TEOS solution prepared in ethanol with a final concentration of 100×10^{-3} M. The mixture was left under mild stirring overnight. The final thickness of the silica-shell coating was 30 ± 3 nm. Finally, the obtained AuNR@SiO_2 were washed to eliminate unreacted products, three times with methanol and three times with DMF, redispersed in 2 mL DMF, and finally, stored in a refrigerator until used.

Synthesis of AuNR@SiO_2@UiO-66 Composite Microbeads: The AuNR@SiO_2@UiO-66 microbeads were synthesized using a slightly modified version of a previously reported spray-drying method.[40] Briefly, terephthalic acid (1 mmol, 166 mg), glacial acetic acid (4 mL), the dispersion of AuNR@SiO_2 particles in DMF (2 mL), and a 70% (w/w) solution of zirconium (IV) propoxide (Zr(OPr^n)$_4$) in 1-propanol (1 mmol, 309 μL) were sequentially added to a flask containing 10 mL of DMF. The resulting mixture was injected into a coil-flow reactor (inner diameter: 3 mm) at a feed rate of 2.4 mL min^{-1} at 115 °C. The resulting preheated solution was then spray-dried at 180 °C (flow rate: 336 mL min^{-1}), using a B-290 Mini Spray-Dryer (BÜCHI Labortechnik; spray cap hole diameter: 0.5 mm). The resulting AuNR@SiO_2@UiO-66 microbeads were dispersed in DMF, washed twice with DMF and ethanol, and finally, dried for 12 h at 85 °C under dynamic vacuum overnight. The percentage of AuNR@SiO_2 NPs encapsulated within the microbeads was determined by ICP-MS to be 9% (w/w). To synthesize the pristine

UiO-66 microbeads, the above procedure was repeated without the addition of the AuNR@SiO_2 particles.

Fabrication of Films Containing AuNR@SiO_2@UiO-66 Microbeads: All the films were prepared following a with slightly modified version of a previously reported procedure.[25] To fabricate the films containing AuNR@SiO_2@UiO-66 microbeads at 8%, 25% or 46% (w/w), 25, 75, or 125 mg of the microbeads, respectively, were thoroughly dispersed into 0.125, 0.375, or 0.625 mL of DMF, respectively, and then sonicated for 15 min. Simultaneously, 225, 175, or 125 mg of PVDF, respectively, were dissolved in 1.125, 0.875, or 0.625 mL of DMF, respectively, by heating at 60 °C. For each microbead-loading level, the two solutions were mixed, and then stirred for 20 min, and then the resulting mixture was drop-casted onto a glass surface, and placed inside an oven preheated to 140 °C for 30 min. The resulting films were detached from the glass slide by submerging them in water, and then placed inside an autoclave filled with methanol. After solvent exchange at 85 °C overnight inside the autoclave, the resultant clean films were recovered, and then dried under dynamic vacuum at 85 °C.

Photothermal Activity: The photothermal activity of the synthesized microbeads was confirmed with a thermal camera by irradiating them at 52, 224, or 1000 mW cm^{-2}, which corresponded to a distance between the laser and microbeads of 15, 7, or 2 cm, respectively.

Iodine Uptake: The iodine-adsorption studies were done by combining either 6 mg of microbeads or a 2-cm^2 portion of film, and 10 mg of elemental iodine, into two different glass tubes (previously tared) with one end sealed. Then, the two containers were introduced into a scintillation vial purged with Ar to remove any moisture that could interfere with gravimetric measurements. The vial was then heated to 75 °C inside an oven for 20 h. At different periods of time, a small aliquot of microbeads, or a small piece of the film, were collected from the vial, and the uptake of iodine in each sample was determined by TGA.

Light-Triggered Release of Iodine: In a typical experiment, either 0.3 mg of microbeads or a small piece ($\approx$1 mg) of film loaded with iodine were placed inside a TGA pan, which was then loaded into the TGA analyzer preset to 30 °C. The samples were then left for 10 min to enable stable measurements. Afterwards, the samples were irradiated for 35 min under NIR light at intensities of 52, 224, or 1000 mW cm^{-2}, and loss in weight of each sample was recorded. The recorded weight loss was compared with the total amount loaded and the release percentage calculated. The experiments were repeated three times for each sample.

Stepwise Light-Triggered Release of Iodine by on/off Switching: The on/off switching experiment began with a small piece ($\approx$1 mg) of an iodine-loaded film being placed inside a TGA pan, which was then loaded into a TGA analyzer preset to 30 °C. The sample was then left for 10 min to enable stable measurements. Next, the film was irradiated for 1 min under NIR light at intensities 52 or of 224 mW cm^{-2}, after which point the laser was turned off for 3 min. The weight loss of the sample was continuously recorded throughout the process. This on/off cycle was repeated 50 times.

Antibacterial Activity Assays: The antibacterial activity of UiO-66 microbeads, AuNR@SiO_2@UiO-66 microbeads, and their corresponding composite films was assessed in different experiments. This began with a disk-diffusion experiment, in which cultures of *E. coli* (ATCC 25922) and *S. aureus* (ATCC 25923) were prepared in Luria–Bertani (LB) agar plates, and then incubated at 37 °C for 18 h. Next, bacterial suspensions were prepared with PBS 1× and adjusted at DO$_{550\ nm}$ = 0.2 (equivalent to 10^8 CFU mL^{-1}). The bacterial suspensions were smeared on the LB plates using cotton swabs that had been dipped in the suspensions. Whatman disks (diameter: 6 mm) were aseptically deposited onto the LB agar surface, and UiO-66 microbeads or AuNR@SiO_2@UiO-66 microbeads ($\approx$1–1.6 mg), with or without iodine, were placed over the disks. In the case of the composite films containing AuNR@SiO_2@UiO-66 microbeads at 8%, 25%, or 46% (w/w), with or without iodine, were directly placed on the LB agar surface. Some of these samples were irradiated for 5 min under NIR light at an intensity of 224 mW cm^{-2}. The plates were left for at 4 °C for 1 h, and then incubated at 37 °C for 18 h. Each experiment was done in duplicate.

Next, the antibacterial performance of the composite films upon iodine release through the air via sublimation provoked by the passive or by the active (light-triggered) iodine-release mechanism was ascertained. To this end, each composite film (size: 1 cm^2) containing either 8% or 25% (w/w) AuNR@SiO$_2$@UiO-66 microbeads loaded with iodine was positioned over a plate cover, and then an agar plate inoculated with a bacterial suspension was placed face down on it. The distance between the composite film and the agar plates was fixed to 1.6 cm. Then, three different experiments were performed. In the first one, the two plates were incubated together at 37 °C for 18 h (Figure 6a). In the second experiment, the composite film was irradiated with NIR light (224 mW cm^{-2}) for 5 min, during which time the plates were rotated. Next, the composite film was immediately removed, and the culture agar plate was sealed with parafilm and incubated at 37 °C for 18 h (Figure 6c). Finally, the third experiment was nearly identical to the second one, except that the irradiation step was skipped (Figure 6b). In all the experiments, additional setups using composite films that did not contain iodine, lacking irradiation and/or not including the removal step were employed as controls. In all cases, the plates were examined to detect and measure (diameters) the growth-inhibition zones.

Statistical Analysis: Data from growth-inhibition diameters are expressed as the mean and SD. A repeated measure two-way ANOVA and Tukey's multiple comparisons test were performed as appropriate, using GraphPad Prism version 6.00 (GraphPad Prism).

Supporting Information

Supporting Information is available from the Wiley Online Library or from the author.

Conflict of Interest

The authors declare no conflict of interest.

Data Availability Statement

The data that support the findings of this study are available from the corresponding author upon reasonable request.

[1] COVID Live Update: 174,753,370 Cases and 3,762,987 Deaths from the Coronavirus – Worldometer, https://www.worldometers.info/coronavirus/ (accessed: June **2021**).

[2] H. A. Khan, F. K. Baig, R. Mehboob, *Asian Pac. J. Trop. Biomed.* **2017**, *7*, 478.

[3] E. Bouza, S. Alonso, A. Asensio, G. De Juan, C. G. Lucio, C. Larrosa, J. López-Iglesias, P. Muñoz, R. Sierra, J. Perianes, J. L. De la Serna, E. Palomo, D. Gracia, *Rev. Esp. Quimioter.* **2019**, *32*, 165.

[4] V. Iacovelli, G. Gaziev, L. Topazio, P. Bove, G. Vespasiani, E. F. Agrò, *Urologia* **2014**, *81*, 222.

[5] M. Cloutier, D. Mantovani, F. Rosei, *Trends Biotechnol.* **2015**, *33*, 637.

[6] I. I. Niyonshuti, V. R. Krishnamurthi, D. Okyere, L. Song, M. Benamara, X. Tong, Y. Wang, J. Chen, *ACS Appl. Mater. Interfaces* **2020**, *12*, 40067.

[7] W. Sim, R. T. Barnard, M. A. T. Blaskovich, Z. M. Ziora, *Antibiotics* **2018**, *7*, 93.

[8] U. Kadiyala, N. A. Kotov, J. S. VanEpps, *Curr. Pharm. Des.* **2018**, *24*, 896.

[9] B. Wang, H. Liu, Z. Wang, S. Shi, K. Nan, Q. Xu, Z. Ye, H. Chen, *J. Mater. Chem. B* **2017**, *5*, 1498.

[10] D. Druvari, N. D. Koromilas, V. Bekiari, G. Bokias, J. K. Kallitsis, *Coatings* **2018**, *8*, 8.

[11] H. Deyhle, G. Schulz, B. Müller, R. H. French, R. H. French, M. E. Samberg, N. A. Monteiro-Riviere, S. Lanone, J. Boczkowski, M. S. Kim, K. Park, H. Tanaka, B. M. Finio, M. Karpelson, N. O. Pérez-Arancibia, P. S. Sreetharan, J. P. Whitney, R. J. Wood, H. Schmitz, H. Soltner, H. Bousack, P. Graham, A. Philippides, P. Decuzzi, T.-L. Ren, Y.-F. Wang, Y. Yang, M. Lian, B. Srijanto, P. Mruetusatorn, et al., *Encyclopedia of Nanotechnology*, Springer, Netherlands **2012**.

[12] A. N. Au-Duong, C. K. Lee, *Mater. Sci. Eng., C* **2017**, *76*, 477.

[13] G. Mcdonnell, A. D. Russell, *Clin. Microbiol. Rev.* **1999**, *12*, 147.

[14] H. G. Brittain, *Anal. Profiles Drug Subst. Excipients* **2002**, *29*, 1.

[15] H. Tsuchiya, T. Shirai, H. Nishida, H. Murakami, T. Kabata, N. Yamamoto, K. Watanabe, J. Nakase, *J. Orthop. Sci.* **2012**, *17*, 595.

[16] G. Selvaggi, S. Monstrey, K. Van Landuyt, M. Hamdi, P. Blondeel, *Acta Chir. Belg.* **2003**, *103*, 241.

[17] D. F. Sava, K. W. Chapman, M. A. Rodriguez, J. A. Greathouse, P. S. Crozier, H. Zhao, P. J. Chupas, T. M. Nenoff, *Chem. Mater.* **2013**, *25*, 2591.

[18] D. F. Sava, M. A. Rodriguez, K. W. Chapman, P. J. Chupas, J. A. Greathouse, P. S. Crozier, T. M. Nenoff, *J. Am. Chem. Soc.* **2011**, *133*, 12398.

[19] W. Xie, D. Cui, S. R. Zhang, Y. H. Xu, D. L. Jiang, *Mater. Horiz.* **2019**, *16*, 1571.

[20] B. Valizadeh, T. N. Nguyen, B. Smit, K. C. Stylianou, *Adv. Funct. Mater.* **2018**, *28*, 1870211.

[21] M. H. Zeng, Q. X. Wang, Y. X. Tan, S. Hu, H. X. Zhao, L. S. Long, M. Kurmoo, *J. Am. Chem. Soc.* **2010**, *132*, 2561.

[22] E. M. Mahdi, A. K. Chaudhuri, J. C. Tan, *Mol. Syst. Des. Eng.* **2016**, *1*, 122.

[23] S. Zhou, J. Gao, J. Zhu, D. Peng, Y. Zhang, Y. Zhang, *J. Membr. Sci.* **2020**, *610*, 118219.

[24] K. Tabatabaeian, M. Simayee, A. Fallah-Shojaie, F. Mashayekhi, M. Hadavi, *J. Iran. Chem. Soc.* **2020**, *17*, 2987.

[25] M. Liu, L. Wang, X. Zheng, Z. Xie, *ACS Appl. Mater. Interfaces* **2017**, *9*, 41512.

[26] J. Troyano, A. Carné-Sánchez, D. Maspoch, *Adv. Mater.* **2019**, *31*, 1808235.

[27] L. Wang, P. Chen, X. Dong, W. Zhang, S. Zhao, S. Xiao, Y. Ouyang, *RSC Adv.* **2020**, *10*, 44679.

[28] W. Cai, J. Wang, C. Chu, W. Chen, C. Wu, G. Liu, *Adv. Sci.* **2019**, *6*, 1801526.

**ADVANCED
SCIENCE NEWS**

www.advancedsciencenews.com

**ADVANCED
FUNCTIONAL
MATERIALS**

www.afm-journal.de

[29] S. Diring, A. Carné-Sánchez, J. C. Zhang, S. Ikemura, C. Kim, H. Inaba, S. Kitagawa, S. Furukawa, *Chem. Sci.* **2017**, *8*, 2381.

[30] Y. Ren, H. Liu, X. Liu, Y. Zheng, Z. Li, C. Li, K. W. K. Yeung, S. Zhu, Y. Liang, Z. Cui, S. Wu, *Cell Rep. Phys. Sci.* **2020**, *1*, 100245.

[31] C. C. Epley, K. L. Roth, S. Lin, S. R. Ahrenholtz, T. Z. Grove, A. J. Morris, *Dalton Trans.* **2017**, *46*, 4917.

[32] Y. Da Zhu, S. P. Chen, H. Zhao, Y. Yang, X. Q. Chen, J. Sun, H. S. Fan, X. D. Zhang, *ACS Appl. Mater. Interfaces* **2016**, *8*, 34209.

[33] Y. Li, J. Jin, D. Wang, J. Lv, K. Hou, Y. Liu, C. Chen, Z. Tang, *Nano Res.* **2018**, *11*, 3294.

[34] K. Khaletskaya, J. Reboul, M. Meilikhov, M. Nakahama, S. Diring, M. Tsujimoto, S. Isoda, F. Kim, K. I. Kamei, R. A. Fischer, S. Kitagawa, S. Furukawa, *J. Am. Chem. Soc.* **2013**, *135*, 10998.

[35] T. K. Sau, C. J. Murphy, *J. Am. Chem. Soc.* **2004**, *126*, 8648.

[36] W. Stöber, A. Fink, E. Bohn, *J. Colloid Interface Sci.* **1968**, *26*, 62.

[37] J. G. Hinman, A. J. Stork, J. A. Varnell, A. A. Gewirth, C. J. Murphy, *Faraday Discuss.* **2016**, *191*, 9.

[38] W. C. Wu, J. B. Tracy, *Chem. Mater.* **2015**, *27*, 2888.

[39] Z. Zhang, Z. Chen, S. Wang, F. Cheng, L. Chen, *ACS Appl. Mater. Interfaces* **2015**, *7*, 27639.

[40] G. Boix, J. Troyano, L. Garzón-Tovar, C. Camur, N. Bermejo, A. Yazdi, J. Piella, N. G. Bastus, V. F. Puntes, I. Imaz, D. Maspoch, *ACS Appl. Mater. Interfaces* **2020**, *12*, 10554.

2112902 (12 of 12)